Synthetic Metals 187 (2014) 172–177

Contents lists available at ScienceDirect

Synthetic Metals

journal homepage: www.elsevier.com/locate/synmet

# ITO-free inverted polymer solar cell on metal substrate with top-illumination

En-Chen Chen [a], Pei-Ting Tsai [b], Chia-Ying Tsai [c], Jung-Hao Chang [d], Zheng-Yu Huang [d], Hsin-Fei Meng [b,*], Huang-Ming Chen [e,**], Hao-Wu Lin [d,***], Sheng-Fu Horng [a], Hsiao-Wen Zan [e]

[a] Department of Electrical Engineering, National Tsing Hua University, Hsinchu 300, Taiwan, ROC
[b] Institute of Physics, National Chiao Tung University, Hsinchu 300, Taiwan, ROC
[c] Institute of Photonics Technologies, National Tsing Hua University, Hsinchu 300, Taiwan, ROC
[d] Department of Materials Science and Engineering, National Tsing Hua University, Hsinchu 300, Taiwan, ROC
[e] Department of Photonics and the Institute of Electro-Optical Engineering, National Chiao Tung University, Hsinchu 300, Taiwan, ROC

ARTICLE INFO

*Article history:*
Received 14 July 2013
Received in revised form 19 October 2013
Accepted 24 October 2013
Available online 6 December 2013

*Keywords:*
ITO-free
Top-illuminated
Blade coating
Semi-transparent electrode

ABSTRACT

High-performance polymer solar cells are conventionally fabricated on the rigid and costly indium-tin-oxide (ITO) glass substrates, which are incompatible with the roll-to-roll process with low cost. This study shows that polymer solar cells can be made on ITO-free flexible stainless steel with only a moderate compromise in power conversion efficiency. A blend of poly (3-hexylthiophene) (P3HT) and (6,6)-phenyl-C61-butyric acid methyl ester (PCBM) was used as the active material for the inverted structure. The bottom electrode was an alloy of Al and Au spontaneously formed from a bi-layer during thermal annealing of the active layer. This alloy had a low work function of 3.9 eV, and a high resistance to oxide formation throughout the entire process. Semi-transparent Ag was used as the top electrode. These solar cells on stainless steel had an efficiency of 2.6%. The majority of the loss came from the top electrode transmission at approximately 60%. This all-metal approach makes roll-to-roll polymer cell fabrication possible.


## 1. Introduction

Polymer solar cells have the great advantage of an economical solution process. Power conversion efficiency above 8% has been reported for glass substrates with transparent indium-tin-oxide (ITO) electrodes with bottom sunlight illumination [1]. Rigid glass substrates are incompatible with the roll-to-roll process for high volume production. Therefore, there have been many studies of ITO-free solar cells [2–7]. Favorable efficiency for polymer solar cells has been demonstrated for flexible plastic substrates [8–12]. The barrier for water and oxygen, required to improve the lifetime of organic semiconductor devices, are not sufficient for plastic substrates. Metal substrates have the simultaneous advantages of mechanical flexibility and strong water–gas barrier. Polymer solar cells with top illumination on metal substrates therefore have the potential for roll-to-roll fabrication, in which the active polymer blend layer can be deposited by slot-die coating [9–11] or blade coating [13,14]. Plastic substrates with copper over-layers have been used for polymer solar cells, and have a lower than 0.1% efficiency [15]. However, few other studies are so far focused on the polymer solar cells on metal substrate.

To achieve top illumination on metal substrates, semi-transparent metal [16,17] or a metal grid over the conducting polymer [9–11] can be used for the top electrode. The bottom electrode however presents more challenges. Several metals or their combination with semiconducting metal–oxide [2] form thin insulating oxide layers when an active polymer semiconductor layer is deposited by solution because of the residual oxygen in the glove box. These insulating layers increase the series resistance of the solar cell and reduce efficiency. The commonly used ITO make effective contact with the polymer blend because it is already an oxide. The exposure to a minimal amount of oxygen therefore does not affect the electrical properties. ITO is expensive and should be avoided in the suggested high volume roll-to-roll fabrication process. All-metal device structures with low series resistance are therefore highly desired.

This study we demonstrate that an alloy of Al and Au spontaneously formed during the polymer layer annealing process has low enough work function and high enough oxygen stability for

* Corresponding author. Tel.: +886 5731955.
** Corresponding author.
*** Corresponding author.
*E-mail addresses:* meng@mail.nctu.edu.tw (H.-F. Meng), pchen@mail.nctu.edu.tw (H.-M. Chen), hwlin@mx.nthu.edu.tw (H.-W. Lin).

0379-6779/$ – see front matter © 2013 Elsevier B.V. All rights reserved.
http://dx.doi.org/10.1016/j.synthmet.2013.10.023

the fabrication of inverted polymer solar cells on metal substrates. A bi-layer of Al and Au is initially evaporated, and the two materials subsequently became mixed as the temperature was raised to 140 °C for 20 min for the active layer to anneal. When stainless steel insulated by photoresist was used as the substrate, and the self-formed Al–Au alloy used as the cathode, the top-illuminated polymer solar cell with a poly(3-hexylthiophene) (P3HT) electron donor blended with the (6,6)-phenyl-C61-butyric acid methyl ester (PCBM) electron acceptor has a power conversion efficiency of 2.6% when the blend was spin-coated. In addition, the blend was blade-coated with an efficiency of 2.3%. For the Cr bottom electrode on glass, the efficiency was 2.2% using spin-coating. The results therefore suggest that all-metal ITO-free polymer solar cells on stainless steel substrates have great potential for extremely cost-efficient roll-to-roll production.

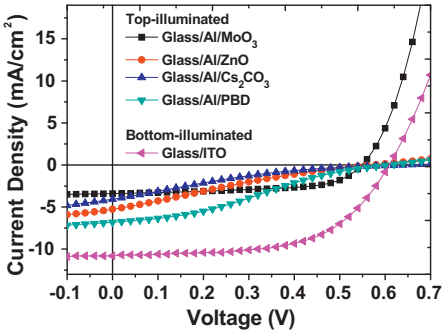


**Fig. 1.** *J–V* characteristics of the normal device structure with the bottom electrode Al/$MoO_3$ and ITO. The *J–V* characteristics of the inverted structure with the bottom electrode of Al/ZnO, Al/$Cs_2CO_3$, and Al/PBD, respectively.

## 2. Experiment

A normal solar cell structure of: glass/Al (100 nm)/$MoO_3$ (35 nm)/P3HT: PCBM/LiF (1 nm)/Al (2 nm)/Ag (15 nm) with top illumination was used and $MoO_3$ was deposited by thermal evaporation below $10^{-6}$ Torr. For the inverted solar cell with ZnO bottom electrodes, the device structure was: glass/Al (100 nm)/ZnO/P3HT: PCBM (250 nm)/PEDOT: PSS (60 nm)/Ag (15 nm). The ZnO precursor was prepared using a sol–gel procedure by dissolving zinc acetate dihydrate ($C_4H_6O_4Zn{\cdot}2(H_2O)$, 99.9%, 2 g), and monoethanolamine ($HOCH_2CH_2NH_2$, 99%, 0.56 g) in anhydrous methanol ($CH_3OH$, >99.8%, 18.2 mL) under vigorous stirring for 12 h to create a hydrolysis reaction and aging. The precursor solution was spin-coated (4000 rpm) onto the Al, sintered in the tube thermal system, annealed at a heating rate of 5 °C $min^{-1}$ to a final temperature of 200 °C, and maintained at this temperature for 1 h before cooling in air to room temperature. The device structure for the inverted solar cell with the Al–Au bottom electrode was stainless steel/photoresist (1.5 μm)/Al (100 nm)/Au (20 nm)/P3HT: PCBM (250 nm)/PEDOT: PSS (60 nm)/Ag (15 nm). The Al–Au alloy spontaneously formed from an initial Al/Au bi-layer during the annealing of the active polymer blend at 140 °C for 20 min. The Cr bottom electrode thickness was 100 nm. The photoresist (EOC130, Everlight Chemical Ind. Corp.) was spin-coated on 7 cm × 8 cm clean stainless steel substrates with a thickness of 75 μm. The wet substrate was pre-baked at 100 °C for 10 min, and then exposed to UV light. The photoresist was used on the stainless steel for two reasons: first, to electrically insulate the steel, and second, to create a smooth surface for the subsequent device fabrication. The surface-planarized film was cured at 230 °C for 30 min. The cured photoresist had a 1.5 μm thickness with a surface roughness of less than 1 nm, measured by atomic force microscopy (AFM). The scrape test was rated 5B for the cured film on stainless steel foil, and was based on the American standard test method (ASTM). A 1:1 weight ratio of the P3HT: PCBM blend was used for the active semiconductor layer. P3HT was purchased from Rieke Metals, and the PCBM was purchased from Nano-C. The solution concentration of the active layer was 1.7 wt.% in dichlorobenzene for spin-coating and 2.5 wt.% in chlorobenzene for blade coating. In all spin-coating samples, the thickness of the active layer was 250 nm with a speed rate of 600 rpm for 40 s, and the wet film was slowly dried for solvent annealing. Fifteen nm of Ag on the conducting polymer poly (3,4-ethylenedioxythiophene): poly-(styrenesulfonate) (PEDOT: PSS) (CLEVIOS™ P, purchased from HC Starck) was used for top illumination for the semi-transparent top electrode. The PEDOT: PSS layer was spin-coated or bladed coated on the active layer using Zonyl FSN (0.2 wt.%) as the processing additive to form a smooth layer with a thickness of 60 nm. It was then soft-baked at 140 °C in the glove box for 20 min. An Ag (15 nm) semi-transparent electrode was formed on the top of active layer by thermal evaporation. The active area of the device was 4 $mm^2$. All device details of the experimental are listed specifically in Table 3. All the devices were packaged using a UV-cured sealant (Everwide Chemical Co., Epowide EX), and a cover glass under the dry nitrogen atmosphere after fabrication, and measured in the ambient environment. The solar cell characteristics of the power conversion efficiency (PCE) were measured under AM 1.5 solar simulator (100 mW/$cm^2$) (XES-301S, SAN-EI). The external quantum efficiency (EQE) was defined as the average number of photo-generated charge carriers contributing to the current per incident photon. It was measured using a lock-in amplifier under short-circuit conditions while the devices were illuminated by monochromatic light from a 250W quartz–tungsten–halogen lamp (Osram) passing through a monochromator (Spectral Products CM110). Calibration of the incident light was performed with a mono-crystalline silicon diode. In order to avoid the overtone effect of the monochromator, we use a high-pass filter to remove the wavelength lower 560 nm. The transmission ratio of various thicknesses of Ag films, ITO, and PEDOT: PSS were measured using a UV–vis spectrophotometer (HP 8453). The work function of the Al–Au alloy and the initial Al/Au bi-layer was measured with a photoelectron spectrum using a surface analyzer model (AC-2, RIKEN KEIKI) for photoemission in air.

## 3. Results and discussion

Before the main results of the Al–Au alloy bottom electrode experiment can be discussed, it is necessary to first explain why common electrodes cannot be used for metal substrates. The Al/$MoO_3$ anode has been known to provide a similar hole injection quality and overall device performance to ITO in OLED. Before presenting the main results on Al–Au alloy we first study some alternative electrodes for comparison. The first is $MoO_3$ with the structure glass/Al (100 nm)/$MoO_3$ (35 nm)/P3HT: PCBM (250 nm)/LiF (1 nm)/Al (2 nm)/Ag (15 nm). This type of normal cell device with an Al/$MoO_3$ anode performed particularly poorly, as illustrated in Fig. 1. Specially, the short circuit current density $J_{sc}$ was below 4 mA/$cm^2$. The dark current density under enough forward bias was even higher than with the ITO anode case, suggesting that the Al/$MoO_3$ anode had low or no hole injection barrier under a high bias for OLED, but had a considerable contact barrier for hole collection under a low bias in the solar cell. PEDOT: PSS was inserted between the $MoO_3$ and the blend in the above normal structure. However, the efficiency decreased further to 0.44%. The bottom electrode of Al/$MoO_3$ was therefore ruled out for the high performance solar cell. The results of the devices are listed in Table 1.

The possibility of an inverted solar cell structure with commonly used ZnO as the bottom cathode was then investigated. The device structure was glass/Al (100 nm)/ZnO/P3HT: PCBM

**Table 1**
The power conversion efficiencies of the normal device structure with the bottom electrode Al/$MoO_3$ and the inverted structure with the bottom electrode of Al/ZnO, Al/$Cs_2CO_3$, and Al/PBD, respectively (The *J*–*V* characteristics are shown in Fig.1).

| Device | PCE (%) |
|---|---|
| 1. Glass/Al/$MoO_3$/P3HT: PCBM/LiF/Al*/Ag | 0.44 |
| 2. Glass/Al/ZnO/P3HT: PCBM/PEDOT: PSS/Ag | 0.67 |
| 3. Glass/Al/$CS_2CO_3$/P3HT: PCBM/PEDOT: PSS/Ag | 0.42 |
| 4. Glass/Al/PBD/P3HT: PCBM/PEDOT: PSS/Ag | 1.20 |

(250 nm)/PEDOT: PSS (60 nm)/Ag (15 nm), again with top illumination. The zinc oxide layer was formed using a sol–gel process from its precursor. The sol–gel process with a curing temperature of 200 °C was completed on the glass/Al substrate. This inverted solar cell with a PEDOT: PSS/Ag top electrode had an efficiency of only 0.67% with top illumination as illustrated in Fig. 1, and was probably because of the formation of an aluminum oxide layer during the curing process. ZnO was replaced by $Cs_2CO_3$ of 5 nm (spin coating) and 2-(4-biphenylyl)-5-(4-tert-butylphenyl)-1,3,4-oxadiazole (PBD) of 3 nm (spin coating), resulting in an efficiency of 0.42% and 1.2%. The poor performance was because of the high reactivity of Al in the standard glove box conditions of $Cs_2CO_3$ and PBD provided efficiency above 3% if deposited onto ITO [19,20].

The bottom cathode of the Al–Au alloy with a top anode of PEDOT: PSS/Ag was then investigated. The inverted solar cell structure was: stainless steel/photoresist (1.5 μm)/Al (100 nm)/Al–Au alloy (20 nm)/P3HT: PCBM (250 nm)/PEDOT: PSS (60 nm)/Ag (15 nm), as illustrated in Fig. 2(a). If no reaction occurred between Al and Au, the bottom electrode had a work function of approximately 5 eV for Au, which was almost the same as that of PEDOT: PSS. Consequently there would be no built voltage and $V_{oc}$ was nearly zero. Al and Au became mixed when the active blend layer is annealed at 140 °C for 20 min. The original purpose of this step was to expel any solvent, and enhance the donor–acceptor phase separation. However, it also changed the color of the bottom electrode from the gold to purple, color as shown in Fig. 3(a). This was probably the result of inter-diffusion between the Al and Au atoms. This purple alloy had two remarkable properties. First, it was highly resistive to oxygen, and the device performance remained constant using the alloy exposed to the air for a week, which was in sharp contrast to Al, which oxidized immediately after evaporation, even in the glove box. In fact, without the Au layer the efficiency was as low as 1.2%. Secondly, the purple alloy had a work function close to that of pure Al. Photoemission in air was performed for Au and the Al/Au alloy, after the 140 °C annealing, as illustrated in Fig. 3(b). The work function of the Au was 4.74 eV, and the work function of the Al/Au alloy was reduced to 3.87 eV. These values were consistent with the Au work function of 5.1 eV and 4.78 eV in high vacuum and air, respectively. The Al reported equally consistent work functions of 4.2 eV in high vacuum and 3.6 eV in air [21,22]. The alloy therefore had the advantage of the low work function of Al but did not have the same high oxygen reactivity problems as Al. The scanning electron

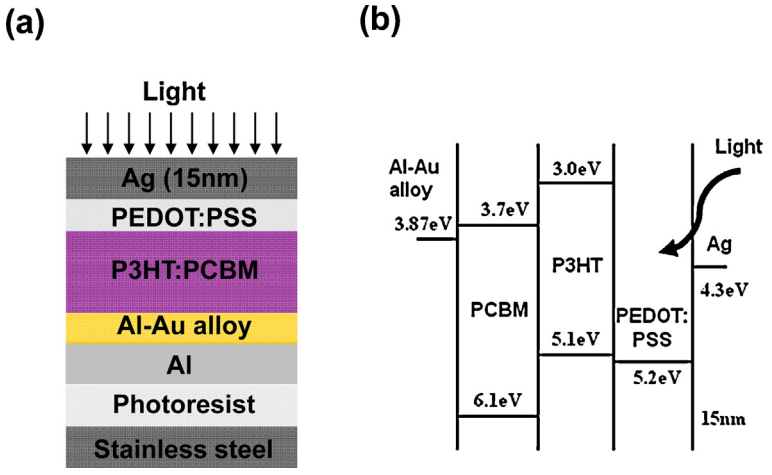


**Fig. 2.** (a) The device structure of the top-illuminated polymer solar cell on the stainless steel substrate. (b) The energy levels of the top-illuminated polymer solar cell.

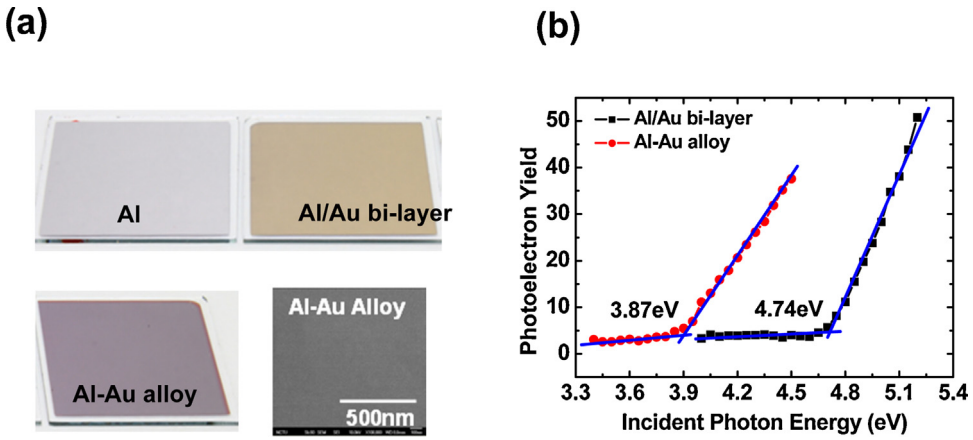


**Fig. 3.** (a) The photographs of the Al, Al/Au bi-layer (top side), and the photographs and SEM images of the Al–Au alloy (bottom side). (b) The photo-emission spectrum measured by a surface analyzer model for the Al/Au bi-layer and the Al–Au alloy.

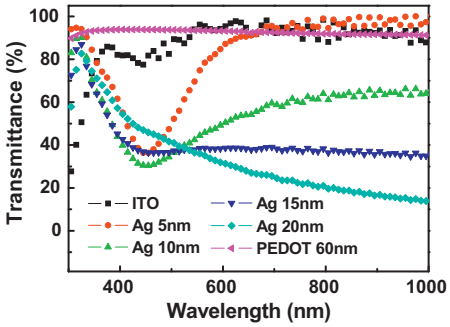


**Fig. 4.** The optical transmittance of semi-transparent Ag films (from 5 nm to 20 nm), PEDOT: PSS (60 nm) and ITO.

microscope (SEM) image of the Al–Au alloy is indicated in Fig. 3(a). The surface morphology of the Al–Au alloy was relatively smooth, diminishing the possibility of shunt leakage. The energy levels of the solar cell are presented in Fig. 2(b).

For top illumination the metal had to be semi-transparent and a trade-off was necessary between the transmittance and the sheet resistance. For the inverted device, a structure of: stainless steel/photoresist/Al/Al–Au alloy/P3HT: PCBM/PEDOT: PSS/Ag, (PEDOT: PSS)/Ag was used as the top anode. The transmission spectra for the semi-transparent top Ag electrode for various thicknesses are indicated in Fig. 4. As expected, the transmittance reduced with thickness, and for 15 nm the transmittance was approximately 40% in the main P3HT absorption spectral range of 450–650 nm. The near perfect transmittance of PEDOT: PSS and ITO are illustrated for comparison. The characteristics of the devices with the Ag electrode versus thickness are shown in Fig. 5(a). The EQE spectrum of 15 nm thickness is illustrated in Fig. 5(b). A crucial observation was that the deviation between the measured $J_{sc}$, and the calculated $J_{sc}$ from the EQE spectra were within 3%. Ag of 15 nm, and this was therefore used as the optimal thickness in the data.

The plain glass that was deposited with thick opaque metal as a model for the metal substrate was used first. The device structure was: metal substrate (Al–Au alloy, Al/Au or Cr)/P3HT: PCBM/PEDOT: PSS/Ag. The active blend of 250 nm was spin-coated in dichlorobenzene. The solar cell performance is illustrated in Fig. 6(a). Because enough difference existed between the work functions of the two electrodes, the device indicated $V_{oc}$ of 0.57 V, and the power conversion had an efficiency of 2.6% with top illumination. This was a far superior result than the $MoO_3$ and ZnO

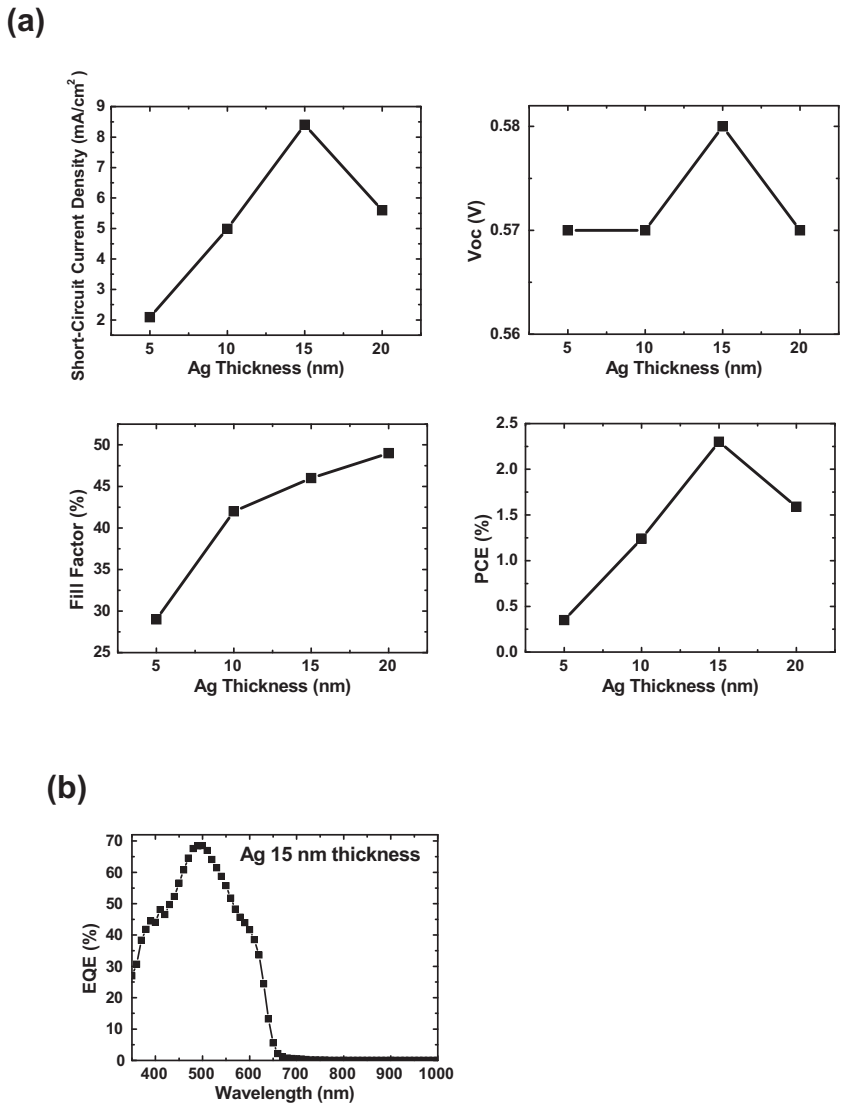


**Fig. 5.** (a) The devices characteristics, and (b) the EQE spectrum of device with Ag 15 nm thickness.

**Table 2**
Photovoltaic parameters for top-illuminated polymer solar cell on stainless steel substrate by spin-coating and blade-coating. (The *J–V* characteristics are shown in Fig.6).

| Device | $J_{sc}$ (mA/cm$^2$) | $V_{oc}$ (V) | Fill factor (%) | PCE (%) |
|---|---|---|---|---|
| 1. Alloy/blend (spin)/PEDOT: PSS/Ag | 9.06 | 0.58 | 50 | 2.6 |
| 2. Al/Au/blend (spin)/PEDOT: PSS/Ag | 5.11 | 0.26 | 33 | 0.4 |
| 3. Cr/blend (spin)/PEDOT: PSS/Ag | 8.09 | 0.58 | 48 | 2.2 |
| 4. Alloy/blend (blade)/PEDOT: PSS/Ag | 8.77 | 0.57 | 47 | 2.3 |

**Table 3**
All device details of the experimental are listed.

| Layers | Thickness (nm) | Deposition |
|---|---|---|
| Al | 100 | Thermal evaporation |
| P3HT: PCBM | 250 | 1.7 wt.% (spin), 600 rpm 40 s and annealing 140 °C 20 min |
| LiF | 1 | Thermal evaporation |
| Al* | 2 | Thermal evaporation |
| Ag | 15 | Thermal evaporation |
| PEDOT: PSS | 60 | 0.2 wt.% (spin), 2000 rpm 40 s and soft-baked 140 °C 20 min |
| $MoO_3$ | 35 | Thermal evaporation |
| ZnO | 30 | Sol–gel process, 4000 rpm 40 s (spin), and cure 200 °C 1 h |
| $CS_2CO_3$ | 5 | 0.2 wt.% (spin), 2000 rpm 40 s |
| PBD | 3 | 0.2 wt.% (spin), 4000 rpm 40 s |
| Au | 100 | Thermal evaporation |

samples provided, and their 2.6% of power conversion efficiency was close to the highest value expected for top illumination, considering the 4% efficiency for bottom illumination devices, and the 40% transmittance of the top electrode. When the blend was dried in vacuum at room temperature, the alloy did not form, the $V_{oc}$ reduced to 0.26 eV, and the efficiency dramatically reduced to 0.4%, as shown in Fig. 6(a). This was to be expected for a device with almost symmetric work functions. By comparing the dark current characteristics (Fig. 6(b)) between these two devices, an enhanced rectification ratio of the Al–Au alloy device was observed ($5.9 \times 10^4$ for the Al–Au alloy versus 51.0 for the Al/Au bi-layer). This result indicated that the Form level of the Al–Au alloy was closer to the PCBM conduction band than the Al/Au bi-layer. When the Al–Au alloy was replaced by another stable metal of Cr, the efficiency was 2.2% (Fig. 6(a)), which was consistent with the previous report on glass substrates [23]. Finally, to simulate the future roll-to-roll fabrication, stainless steel was used as the substrate and both the P3HT: PCBM blend and PEDOT: PSS were deposited by blade-coating. The device efficiency was 2.3%, as indicated in Fig. 6(a). The results of the devices are tabled listed in Table 2. The slight difference between the spin-coated and blade-coated efficiency may have been the result of the variation of the blend thickness. Even though the efficiency of the top illuminated solar cell was lower than the bottom illuminated cell by approximately 30% in the small area because of the limited transmittance of the top electrode, in the large area, the former may have exceed the latter because of the potentially considerably lower sheet resistance. In the conventional bottom illuminated device, the photo-current collection was ultimately limited by the ITO sheet resistance and the efficiency dropped to lower than 1% in large areas, despite small area efficiency above 4%. By contrast the bottom electrode of the opaque Al has extremely low sheet resistance in the top illuminated devices. The sheet resistance of the semi-transparent top electrode could be enhanced by the deposition of an additional metal grid [9–11] over the thin transparent metal. The large area efficiency for the top illuminated device on the metal substrate therefore had the potential for similar efficiency in both the small and large areas, which is crucial for solar cell applications.

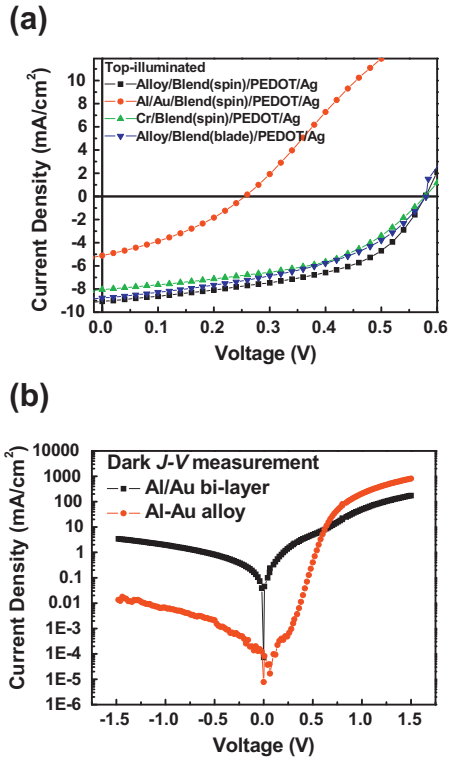


**Fig. 6.** (a) *J–V* characteristics of the top-illuminated polymer solar cell on stainless steel substrate by spin coating and blade coating. (b) The dark current characteristics of Al/Au bi-layer and Al–Au alloy.

## 4. Conclusion

The polymer solar cell with a P3HT donor, and PCBM acceptor had an efficiency of 2.3% in flexible stainless steel with top illumination from the semi-transparent electrode. Only metals were used for the bottom anode and the top cathode, and the entire devices were built without using any of the costly ITO. An alloy of Al and Au spontaneously formed during the active layer annealing, and combined the benefits of low work function and high resistance to oxidation, which were desired for the bottom electrode. Blade coating was applied for all the organic layers. This type of fabrication on metal substrate could easily be implemented in roll-to-roll processes in high volumes. Even though gold is a precious metal the cost is now lower than indium. More works are to be done for the use for low-cost metals.

## Acknowledgments

This work is supported by the National Science Council of Taiwan under Contract Nos. 98-2112-M-007-028-MY3, 99-2628-M-009-001 and the Ministry of Economic Affairs of Taiwan under Contract No. 99-EC-17-A-07-S1-157.

## References

[1] Z. He, C. Zhong, X. Huang, W.Y. Wong, H. Wu, L. Chen, S. Su, Y. Cao, Adv. Mater. 23 (2011) 4636.
[2] S. Wilken, T. Hoffmann, E. von Hauff, H. Borchert, J. Parisi, Sol. Energy Mater. Sol. C 96 (2012) 141.
[3] M. Neophytou, F. Hermerschmidt, A. Savva, E. Georgiou, S.A. Choulis, Appl. Phys. Lett. 101 (2012) 193302.
[4] Y. Jin, J. Feng, Y.-H. Wang, M. Xu, T. Lan, Y.-G. Bi, Q.-D. Chen, H.-Y. Wang, H.-B. Sun, IEEE Photon. J. 4 (2012) 1737.
[5] Y. Galagan, B. Zimmermann, E.W.C. Coenen, M. Jørgensen, D.M. Tanenbaum, F.C. Krebs, H. Gorter, S. Sabik, L.H. Slooff, S.C. Veenstra, J.M. Kroon, R. Andriessen, Adv. Energy Mater. 2 (2012) 103.
[6] Y. Galagan, E.W.C. Coenen, S. Sabik, H.H. Gorter, M. Barink, S.C. Veenstra, J.M. Kroon, R. Andriessen, P.W.M. Blom, Sol. Energy Mater. Sol. C 104 (2012) 32.
[7] D. Angmo, F.C. Krebs, J. Appl. Polym. Sci. 129 (2013) 1.
[8] Y. Galagan, J.E.J.M. Rubingh, R. Andriessen, C.C. Fan, P.W.M. Blom, S.C. Veenstra, J.M. Kroon, Sol. Energy Mater. Sol. C 95 (2011) 1339.
[9] M. Manceau, D. Angmo, M. Jogensen, F.C. Krebs, Org. Electron. 12 (2011) 566.
[10] F.C. Krebs, Org. Electron. 10 (2009) 761.
[11] F.C. Krebs, S.A. Gevorgyam, J. Alstrup, J. Mater. Chem. 19 (2009) 5442.
[12] S.K. Hau, H.L. Yip, J. Zou, A.K.Y. Jen, Org. Electron. 10 (2009) 1401.
[13] Y.H. Chang, S.R. Tseng, C.Y. Chen, H.F. Meng, E.C. Chen, S.F. Horng, C.S. Hsu, Org. Electron. 10 (2009) 741.
[14] S.R. Tseng, H.F. Meng, K.C. Lee, S.F. Horng, Appl. Phys. Lett. 93 (2008) 153308.
[15] F.C. Krebs, Sol. Energy Mater. Sol. C 93 (2009) 1636.
[16] J. Meiss, M. Furno, S. Pfuetzner, K. Leo, M. Riede, J. Appl. Phys. 107 (2010) 053117.
[17] A. Bedeloglu, A. Demir, Y. Bozkurt, N.S. Sariciftci, Renew. Energy 35 (2010) 2301.
[19] H.H. Liao, L.M. Chen, Z. Xu, G. Li, Y. Yang, Appl. Phys. Lett. 92 (2008) 173303.
[20] A. Colsmann, J. Junge, T. Wellinger, C. Kayser, U. Lemmer, Proc. SPIE 6192 (2006) 619220.
[21] M. Uda, Jpn. J. Appl. Phys. 24 (1985) 284.
[22] D.E. Eastman, Phys. Rev. B2 (1970) 1.
[23] B. Zimmermann, U. Wurfel, W. Niggemann, Sol. Energy Mater. Sol. C 93 (2009) 491.

## Further reading

[18] A.K.K. Kyaw, X.W. Sun, C.Y. Jiang, G.Q. Lo, D.W. Zhao, D.L. Kwong, Appl. Phys. Lett. 93 (2008) 221107.